DOI: 10.13009/EUCASS2023-031
Aerospace Europe Conference 2023 – 10TH EUCASS – 9TH CEAS

Investigation of Different Porous Injection Technologies in a LOX/CH4 Rocket Combustor with Optical Access at Sub-, Trans- and Supercritical Conditions

Ivens D. Hoffmann⋆*, Dmitry I. Suslov*†*, Jan Martin*†*, Wolfgang Armbruster*†*, Jan C. Deeken*† *and Justin Hardi*†
⋆ *Institute of Space Systems - Stuttgart University, Pfaffenwaldring 29, 70569 Stuttgart, Germany*
† *Institute of Space Propulsion, German Aerospace Center (DLR), 74239 Hardthausen, Germany*
⋆ivens.hoffmann@dlr.de
⋆Corresponding author

Abstract

For the performance and stability of liquid propellant rocket engines, injector behavior is of utmost importance. A major problem is achieving an effective chemical reaction and a highly efficient homogeneous mixture of fuels with a minimum chamber length. These processes are also crucial in many other modern combustion systems such as chemical industrial plants, heating systems, and engines, which lead to extremely high requirements for the injection equipment. This article presents a concept for an injection system based on the application of different porous materials and oxidizer injectors. The system has been designed based on DLR Lampoldshausen's heritage within porous injection technologies and its possible future use at the DLR LUMEN Technology Demonstrator. The setup has been successfully implemented and operated under sub-to-supercritical pressure conditions (tested from 35 to 65 bar), with respect to the critical pressure of oxygen, using the penta-injector research combustor. Optical investigations of the near-injector combustion and flow field behavior for different penta-injector elements were conducted. Fuel was injected through a metallic mesh (Rigimesh®) or sinter bronze (CA-100). As for the oxygen injector, three different variations were tested: a conventional axial injector, a pentagon pattern riffling injector, and a helical swirl injector. The latter two were manufactured using Additive Layering Manufacturing (ALM).

1. Introduction

Liquid oxygen (LOX) and liquid hydrogen (LH2) have long been utilized as propellants for liquid propellant rocket engines (LPREs) in the USA and Europe. This is attributed to their high specific impulse, which surpasses that of other fuels. However, there is currently a growing trend towards the exploration of new fuels that are more cost-effective and easier to handle. Liquid methane (CH4) is one such fuel, particularly in light of the upcoming goal of landing on Mars.

Injectors play a critical role in LPREs as they directly impact flame anchoring, combustion stability, system pressure, and combustor length. Consequently, the search for improved injector types is of great interest.

At the German Aerospace Center (DLR) in Lampoldshausen, Germany, a novel porous injector type called the Advanced Porous Injector (API) has already undergone testing with LOX/LH2. The results have demonstrated effective atomization, thereby offering the potential to reduce the length of the combustor chamber.[3]

The utilization of the Advanced Porous Injector (API) as an injector for CH4 holds potential for yielding interesting results. However, modifications are necessary for LOX injectors to enhance atomization, considering the slower flame propagation velocity and higher density of CH4 compared to LH2.

Subscale experiments with optical access provide the best approach to observe flame anchoring, as well as the atomization and combustion processes in the vicinity of the injector tip. The DLR's optically accessible rocket combustor model "C" (BKC) is a well-known and commonly used subscale model specifically designed for this purpose.[5,13]

This study presents experiments conducted using the DLR optically accessible rocket combustor model "C" (BKC). The experiments involved the use of two different porous materials as fuel injectors and three different types of injectors for the oxidant side. The oxidant/fuel combination utilized was liquid oxygen (LOX) and compressed-natural-gas/liquefied-natural-gas (CNG/LNG). To gain insights into the combustion and atomization processes, high-speed imaging in the ultraviolet wavelength regime (OH*) and Shadowgraphy techniques were employed.

DOI: 10.13009/EUCASS2023-031

The first part of the presentation will delve into the theory behind both porous and swirl injectors. Subsequently, the experimental setup of the combustor chamber, including the injectors, will be showcased. Finally, the findings obtained from conventional and optical data will be presented and discussed.

2. Theory

The flow through a porous medium is inherently complex, making it challenging to analyze using analytical approaches. Currently, the most effective approach is empirical or semi-empirical, relying on universal constants and easily measurable properties of both the porous medium and the flowing fluid.

In the context of flow through porous media, it is desirable to predict the flow rate achievable with a given energy input, typically measured as pressure drop (δP), or to be able to predict the pressure drop required to achieve a specific flow rate.

The modeling of Newtonian fluid flow through porous media has been studied since 1856, with Henry Darcy demonstrating a linear relationship between the flow rate through a porous bed and the pressure drop, as shown in Equation 1. This relationship is based on the conservation of momentum.[9]

$$\delta P = -\frac{\mu_f}{K} u_D \tag{1}$$

In Darcy's Law, the pressure loss (δP) is determined by the dynamic viscosity (μ_f), specific permeability (K), and fluid velocity (u_D). However, it is important to note that Darcy's Law is only applicable for lower flow speeds, corresponding to small Reynolds numbers. At high flow speeds, inertial contributions become significant, necessitating the inclusion of additional terms in the equation.

To address these inertial effects, researchers have developed various models. One widely used method, known as Forchheimer's equations, was introduced in 1901.[8,10] Forchheimer's equations provide a means to model the inertial contributions in high-speed flows, extending the applicability of the analysis beyond the limitations of Darcy's Law.

Equation 2 combines both the Darcy term, which accounts for viscosity and permeability, and the Forchheimer term, which incorporates the inertial effects of the flow. The Forchheimer coefficient represents the resistance to flow caused by inertial effects, and the fluid density (ρ) is also included to account for the mass of the fluid.

$$\delta P = -\frac{\mu_f}{K} u_D - \frac{C_f}{\sqrt{K}} \rho u_D^2 \tag{2}$$

Expanding upon Equation 1, the inclusion of Forchheimer's equations introduces the Forchheimer coefficient (C_f) and fluid density (ρ).

$$\alpha = K \tag{3}$$

$$\beta = \frac{\sqrt{K}}{C_f} \tag{4}$$

$$\delta P = -\frac{\mu_f}{\alpha} u_D - \frac{\rho}{\beta} u_D^2 \tag{5}$$

The commonly used representation of Forchheimer's equation is shown in Equation 5, which incorporates the implementation of Equations 3 and 4 into Equation 2. The values of α and β are specific to the porous medium being considered and can be found in catalogs or determined through experimental or numerical methods. These values are crucial in the design process for accurately predicting the pressure drop and flow rate in high-speed flows through porous media.

The major limitation of Forchheimer's Equation is the lack of parameters to define the porous medium. Therefore, the parameters α and β must be a function of the specific media rather than universal constants. α is responsible for the viscous-dominated flow part, while β accounts for the inertial-dominated part. Both α and β need to be empirically established for each individual medium. To overcome this issue, Ergun's equation was developed in 1952.[6] The idea behind Ergun's equation was to incorporate direct porous medium parameters, such as porosity (ϵ) and the equivalent diameter (D), as shown in Equation 6.

$$\delta P = -\mu \frac{150(1-\epsilon)^2}{\epsilon^3 D^2} u_D - \frac{1,75\rho(1-\epsilon)}{\epsilon^3 D} u_D^2 \tag{6}$$

It was later noted that the surface quality of the porous surface significantly influences the pressure loss. As a result, two sets of values can be used in the previous equation. If the surface is smooth (A = 180 and B = 1.8), the

DOI: 10.13009/EUCASS2023-031

equation remains similar to its original form. However, if the surface is rough (A = 180 and B = 4.0), a modified equation is utilized, as shown in Equation 7.

$$\delta P = -\mu \frac{A(1-\epsilon)^2}{\epsilon^3 D^2} u_D - \frac{B\rho(1-\epsilon)}{\epsilon^3 D} u_D^2 \tag{7}$$

Swirl injectors are widely used in aerospace applications nowadays due to their excellent mixture capabilities for high-energy fuels. There are two types of swirl injectors: one uses tangential holes at the base of the injector to create a vortex, while the other utilizes swirler inserts, which are commonly used for liquid fluids.

In this particular case, a helical swirler type was chosen to generate the angular momentum for the oxidizer, considering the small size of the injector and the complexity of manufacturing. For this type of injector, the final cone angle of the spray α in the combustion chamber can be calculated using Equation 8.

$$\alpha = arctan(\frac{w}{u}) = arctan(\frac{3}{2} SN) \tag{8}$$

Where w is the tangential velocity, u the axial velocity of the fluid and SN is the Swirl Number. The Swirl Number (SN) is a dimensionless number that characterizes the rotating flows.[1,2] It can be defined as shown in Equation 9.

$$SN = \frac{G_{tan}}{G_{ax} R} = \frac{\frac{2}{3}\pi R^3 uw}{R\pi\rho R^2 u^2} = \frac{2}{3}\frac{w}{u} = \frac{2}{3}\left[\frac{1-(D_h/D_t)^3}{1-(D_h/D_t)^2}\right] tan(\beta) \tag{9}$$

Where G_{tan} is tangential momentum, G_{ax} is axial momentum, R is the radius of the injector inner wall, D_h is the diameter of the injector inner wall, D_t is the diameter where the fins starts (if a co-axial injector is used), and β is the angle of the swirler fins.

For this research involving swirlers, neglecting friction losses with the injector wall, the final angle of the spray (α) is the same as the angle of the swirler fin itself (β). This correlation can be obtained by combining Equation 8 with equation 9. In this concept, β is set to 45°.

$$\alpha = \beta \tag{10}$$

However, Equation 10 can only be used in swirlers with a constant fin angle (β) along the radius. Due to the nature of the helix form, it is observed that at the center of the swirler ($r_0 = 0$), no angular momentum is achieved, resulting in $\beta = 0°$. Conversely, at the extremities of the insert ($r_1 = 0.75$ in this concept), a maximum momentum can be obtained, corresponding to $\beta = 45°$.

Therefore, to determine an equivalent value for β, interpolation is necessary, as shown in Equation 11

$$\alpha = \beta_{eq} = \frac{\int_{r_0}^{r_1} 2\pi r^2 sin(\beta)}{\pi R^2} \tag{11}$$

3. Experimental Setup

3.1 Combustor

The injectors were tested at the European Science and Technology P8 test bench of the Institute of Space Propulsion at the German Aerospace Center (DLR) in Lampoldshausen. In this particular case, the injector element was integrated into the 50 mm diameter water-cooled rocket combustor "C" (BKC).[4,7,11] The combustor used in the experiment features an optical access near the injector head, measuring 100 mm x 25 mm in size. Figure 1 provides a schematic overview of the experimental setup, showcasing the BKC at the center with quartz windows installed on both sides.

For data analysis, static pressure sensors with a scan rate ranging from 100 to 1000 Hz, dynamic pressure sensors with a scan rate of 100 kHz with a 30 kHz anti-aliasing filter, and K-type thermocouples with a scan rate frequency of 100 Hz were used. These sensors were implemented throughout the entire assembly, including the domes and combustor.

The test sequence, along with all 27 target load points, is illustrated in Figure 2.

DOI: 10.13009/EUCASS2023-031

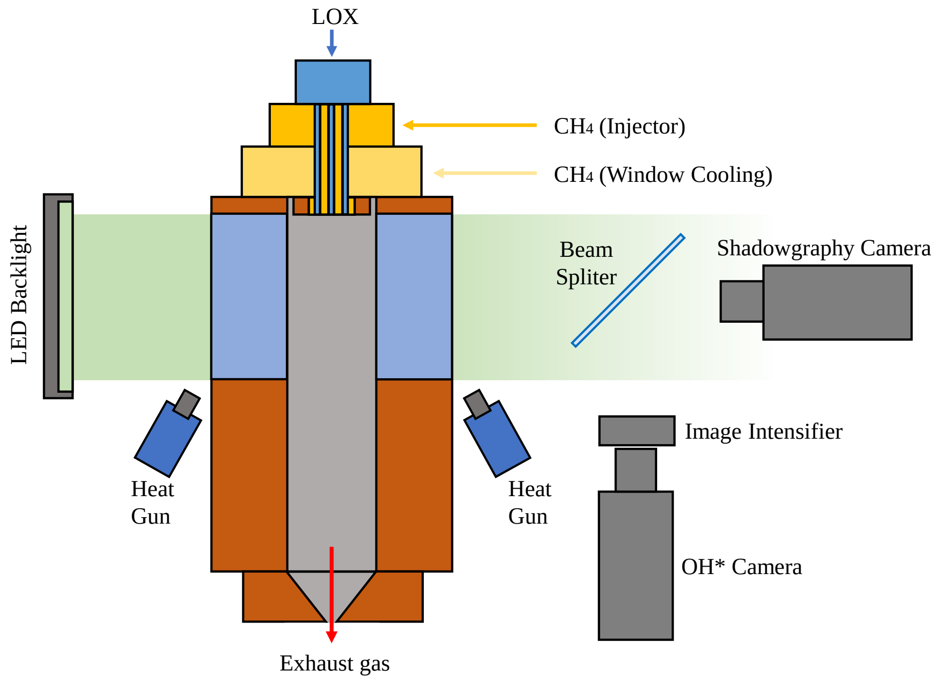

Figure 1: Schematic overview of experimental setup at the P8 test-bench

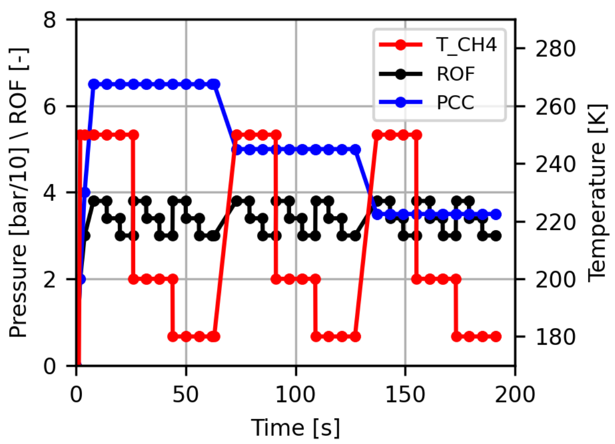

Figure 2: Test sequence tested at the P8 test-bench

3.2 Optical Setup

The entire window was illuminated using a planar LED back-light. On the opposite side, two high-speed cameras were positioned. In line with the optical access, a Photron SA-Z high-speed camera with green and yellow filters were used to record shadowgraphy images, while at a 90-degree angle, a Photron SA-X2 camera with an image intensifier and a 310 +- 3 nm interference filter were used to capture OH*-images. Both cameras recorded at 1000 frames per second (fps). To prevent the windows from freezing and blocking due to atmospheric moisture, two heat guns were employed.

3.3 Injectors

Figure 3 shows the six different injector combinations that generated the data analyzed in this work. For the fuel injector, two different porous materials were used: Sinter Bronze (CA-100) from the company GGT Gleitlage AG and

DOI: 10.13009/EUCASS2023-031

a stainless steel mesh (Rigimesh®) from Pall Corporation. The dimensions and mechanical data of these materials are presented in Table 1.

Table 1: Porous injectors dimensions and mechanical properties

	CA-100	**Rigimesh®**
Outter diameter (mm)	14	14
Thickness (mm)	10	10
Porosity (%)	42	≈37[a]
α (m^2)	200e-12	-[a]
β (m)	150e-7	≈180e-7[a]

[a] data from previous empirical in house tests

For the oxidizer side, three different injectors were tested, as shown in Figure 3. The first injector used was the original axial injector, which had previously demonstrated good results with hydrogen as fuel in the API injector head.[3, 12]The remaining two injectors were designed to increase tangential velocities at the exit of the injector tip. One injector had a riffling design with a pentagon cross-section, while the other had a swirl design with a helical swirler. Both injectors were manufactured using additive layer manufacturing (ALM) due to the complexity of the small injector dimensions. More details about these injectors can be found in Table 2.

Table 2: Oxidant injector dimentions

	Axial	**Riffling**	**Swirl**
Outter diameter (mm)	2,3	2,3	2,3
Inner diameter [a](mm)	1,5	1,4	1,4
Length (mm)	71,8	71,8	71,8
Injector distance X-Axis (mm)	3,5	3,5	3,5
Injector distance Y-Axis (mm)	3,5	3,5	3,5
Angle[b] (°)	-	45	45
Swirler Thickness (mm)	-	-	0,2

[a] Due to ALM manufactuing process the final inner diameter achieved was 1,4 mm instead of the 1,5 mm expected

[b] Angle used for the Helix Swirler and the printing of the Riffling in Z-Axis

4. Results

4.1 Conventional Data

Figure 4 shows that for both porous media, the Forchheimer equation did not produce good results, with deviations ranging from 5% at 75 s to 75% at 90 s time mark. On the other hand, the Ergun's Modified equation provided a relatively good comparison between analysis and test results. The variations in pressure loss were in the range of 2% at 170 s and 30% at 90 s time period.

It is worth noting that for the Ergun's Modified Equation, the approach used for surface roughness was A = 180 and B = 4.0. These parameters were chosen to account for the rough surface quality of the sintered bronze spheres and the metal mesh in the medium.

For the stainless steel mesh, the parameters(α, β and ϵ) were empirically obtained from previous tests conducted at the P8 test-bench. Therefore, a larger deviation could be expected.

Figure 5 shows the effective value in each second from the dynamic pressure in the near injector area for all six cases.

Unfortunately, the combination of axial injectors with the sintered bronze porous plate was not able to generate good atomization. As a result, smooth combustion at supercritical conditions and transcritical conditions could not be achieved. High-frequency (HF) instability occurred, and the test had to be terminated.

DOI: 10.13009/EUCASS2023-031

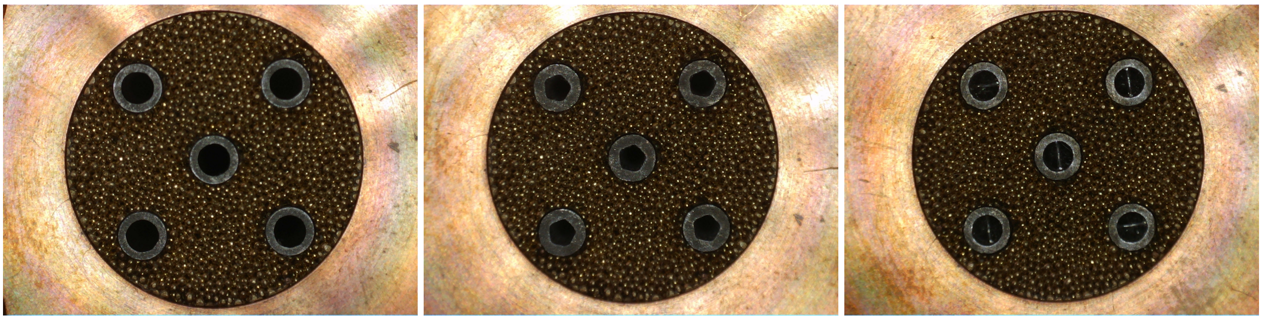

(a) Axial/Sinter Bronze Penta-Injector (b) Riffling/Sinter Bronze Penta-Injector (c) Swirl/Sinter Bronze Penta-Injector

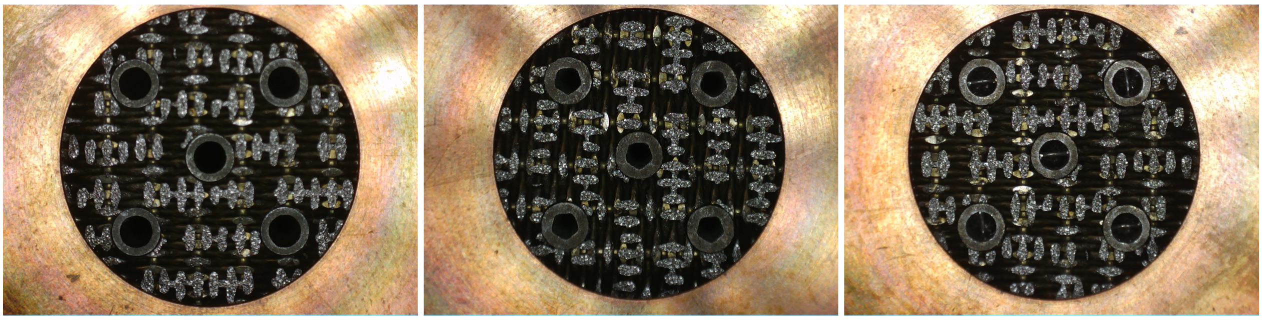

(d) Axial/Stainless-Steel Mesh Penta-Injector (e) Riffling/Stainless-Steel Mesh Penta-Injector (f) Swirl/Stainless-Steel Mesh Penta-Injector

Figure 3: Injector geometry variations

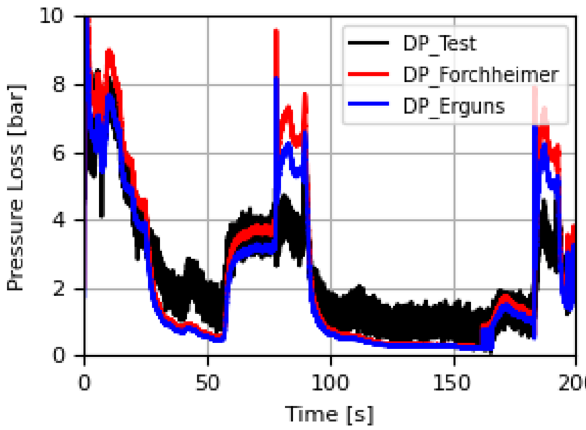

(a) Sinter Bronze as Porous Media

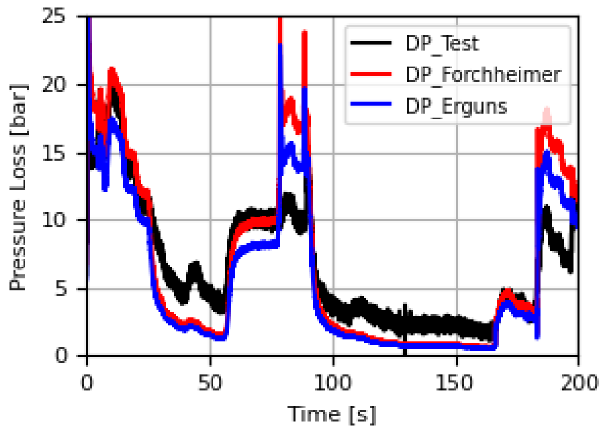

(b) Stainless Steel Mesh as Porous Media

Figure 4: Pressure Drop analysis using Forchheimer- and Erguns-Modified Equations

Similarly, when using the combination of axial injectors with a steel-mesh porous plate, HF instabilities appeared from the beginning of the test. After 48 seconds, the test also had to be terminated.

For the riffling injector with both the sintered bronze and steel-mesh porous media combination, an interesting smooth combustion was observed at supercritical and transcritical conditions. However, during subcritical conditions, some rough combustion could be seen. This effect may be attributed to the lack of shear forces to overcome the surface tension of the fluid, even at the outer annulus of the LOX fluid where the tangential forces are the strongest.

The swirl injectors exhibited the best results among all three types of injectors used for the oxidant type, regardless of the porous medium type. These injectors performed well under all conditions, demonstrating good atomization, particularly in subcritical conditions.

A more detailed explanation of the atomization can be found in the next chapter.

DOI: 10.13009/EUCASS2023-031

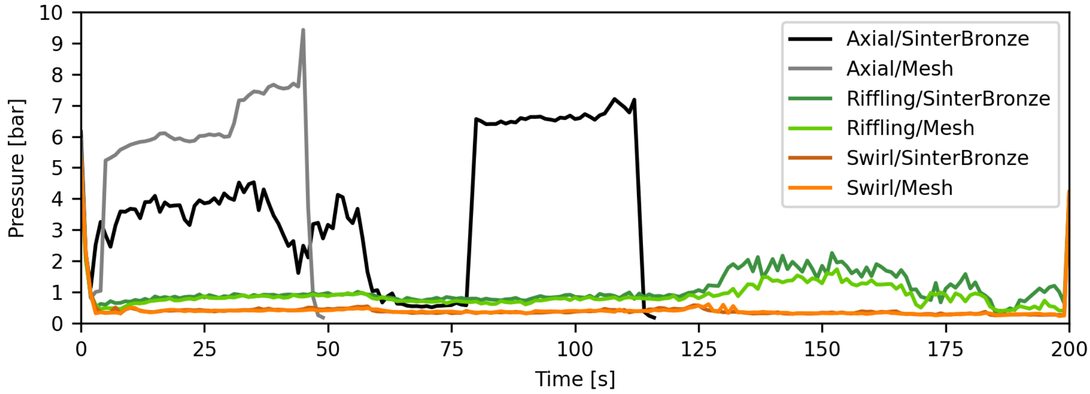

Figure 5: RMS Dynamic Instabilities near the injector area from the six different Injectors

4.2 Optical Data

To investigate the atomization and combustion process in the combustion chamber, shadowgraphy and OH* measurements were used, respectively. The optical data presented in this paper are from the main load point, with a chamber pressure of 65 bar, fuel temperature of 250 K, and an oxygen/fuel ratio of 3,4 (ROF).

As observed in Figure 6, the combination of axial injectors shows that the flame is anchored at the injector tip, but only when using the sintered bronze porous media. In this case, the first combustion region can be clearly identified at approximately 30 mm from the injector face.

For the axial injector with stainless steel mesh, the atomization process was not optimal. As shown in Figure 6 (b) and (d), there was no anchoring from the flame. The shear forces were insufficient to atomize the LOX, and the relative fluid velocities were likely higher than the flame front propagation velocity, resulting in unstable combustion, as depicted in Figure 5. It is also important to note that the axial/mesh injector combination experienced HF instabilities from the beginning of the tests. The cause could be attributed to the mesh pattern or the lack of heat exchange between the mesh and fuel, both of which could exacerbate the combustion dynamics.

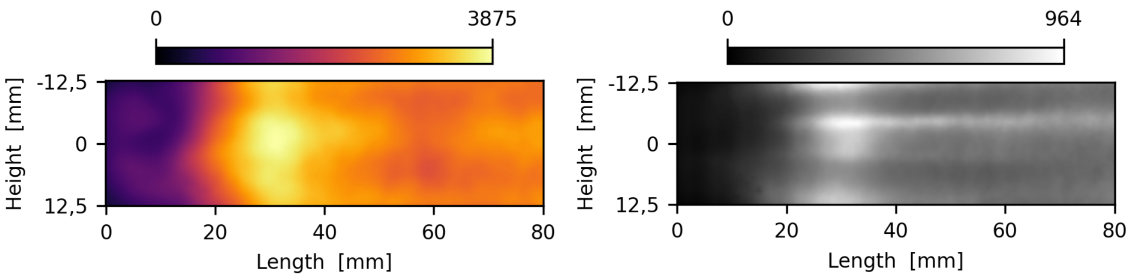

(a) OH* Image.

(b) Shadowgrphy Image.

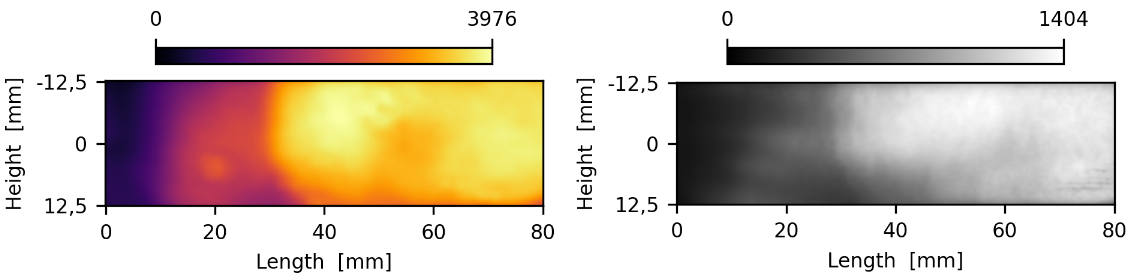

(c) OH* Image.

(d) Shadowgrphy Image.

Figure 6: OH* and Shadowgraphy from Axial/Sinter Bronze (a,b) and Axial/Stainless Steel Mesh Injectors (c,d) for 65 bar combustion chamber pressure, 250 K fuel temperature and 3,4 ROF

For both riffling/porous media tests, a slightly better atomization and therefore combustion were achieved compared to the previous injector combination. Figures 7 (a) and (c)demonstrate that the flame anchored at the injector tip,

DOI: 10.13009/EUCASS2023-031

and in this case, both the sintered bronze and mesh created a stable first combustion zone around the 30 mm mark in the combustion chamber. Figures 7 (b) and (d) exhibit an increase in LOX spray thickness, indicating that the spin of the riffling walls generated a small tangential momentum in the fluid, aiding in the atomization process. From Figure 5 , it can be observed that this effect only applies to the super- and trans-critical regions (65 and 50 bar) where surface tension is not present.

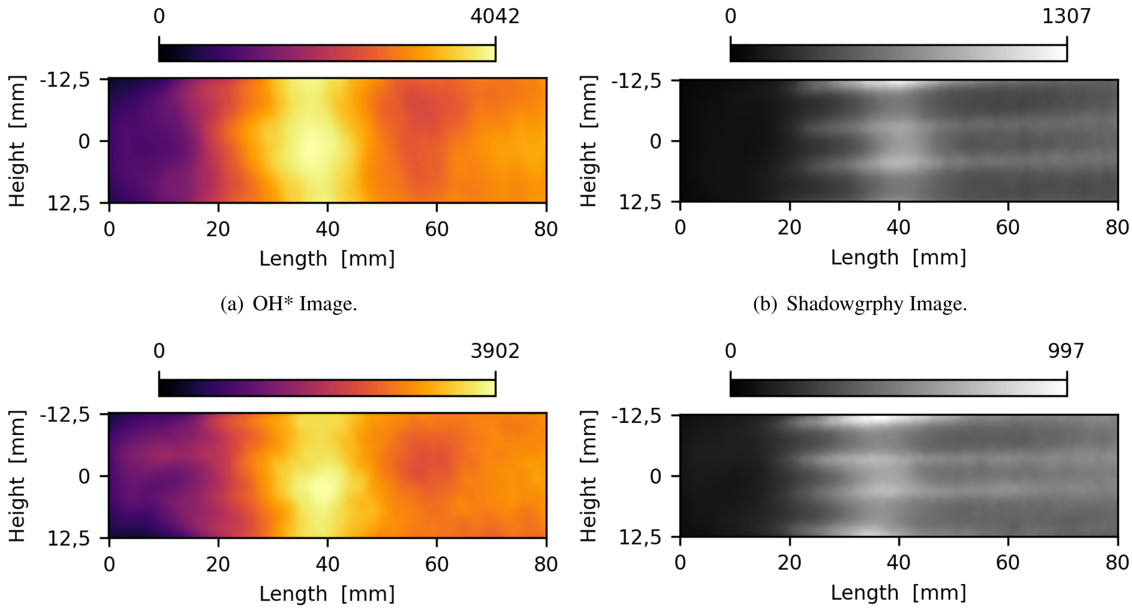

(a) OH* Image. (b) Shadowgrphy Image.

(c) OH* Image. (d) Shadowgrphy Image.

Figure 7: OH* and Shadowgraphy from Riffling/Sinter Bronze (a,b) and Riffling/Stainless Steel Mesh Injectors (c,d) for 65 bar combustion chamber pressure, 250 K fuel temperature and 3,4 ROF

In Figure 8 the atomization (c and d) and combustion process (a and b) from the swirl/porous media injectors can be observed. This combination yielded the best results among all the injector configurations. The implementation of the swirler generated a significant amount of tangential forces, surpassing the riffling injector, thereby enhancing the atomization process, as depicted in Figure 8 (b) and (d). This improvement in atomization reduced the distance of the first combustion region to 20 mm from the faceplate, as shown in Figure 8 (a) and (c). It is important to note that the swirler created higher recirculation zones compared to the other injectors, resulting in less soot formation on the windows. This can be attributed to the higher turbulence in the region, which aids in removing soot from the windows. Additionally, it is worth mentioning that, in this case, the mesh porous media demonstrated better atomization and combustion compared to the sintered bronze media.

5. Conclusion and Outlook

This manuscript presents an experimental study conducted at the P8 test-bench at the Institute of Space Propulsion in Lampoldshausen, Germany. The objective of this test campaign was to investigate the performance of different injector geometry variations using porous media as fuel injectors in a LOX/CH4 combustion chamber. The study utilized sensor and optical analysis techniques to evaluate the atomization performance of the injectors.

The results revealed that the swirl injector exhibited the best atomization performance across all load points, outperforming the other two injectors tested for the oxidizer. Both the sintered bronze and stainless steel mesh porous media demonstrated satisfactory pressure loss and atomization characteristics.

This study represents the initial phase of the development of an 80 mm porous injector head for LOX/CH4. The injector head is currently undergoing testing for a deep throttling liquid rocket engine as part of the future LUMEN Project at the German Aerospace Center in Lampoldshausen.

DOI: 10.13009/EUCASS2023-031

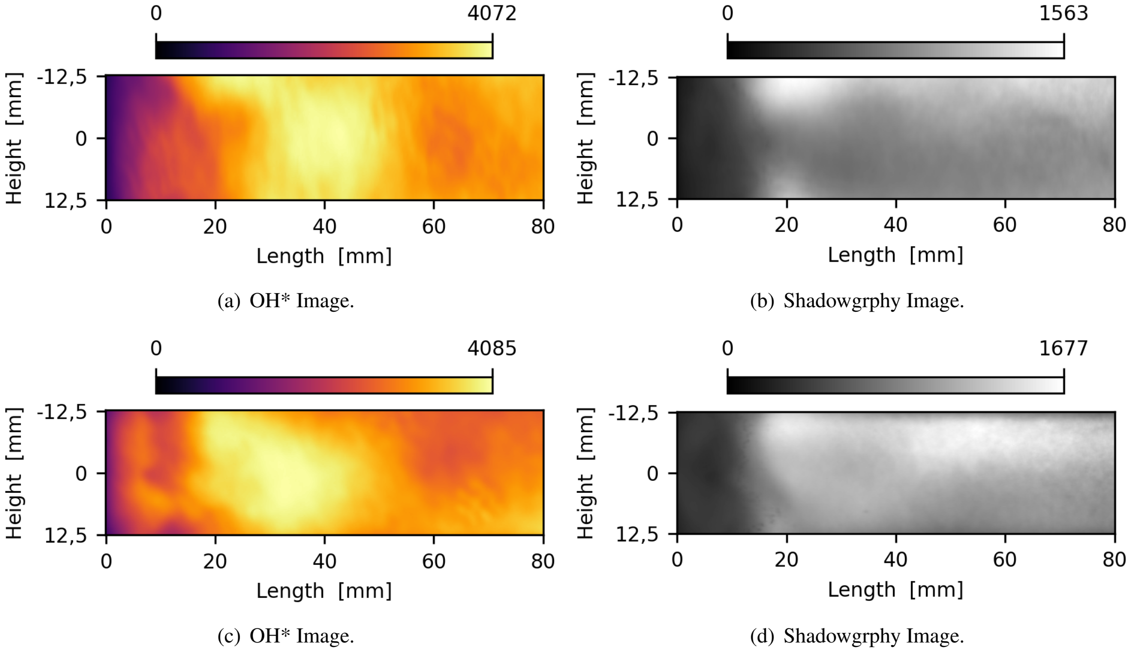

(a) OH* Image.

(b) Shadowgrphy Image.

(c) OH* Image.

(d) Shadowgrphy Image.

Figure 8: OH* and Shadowgraphy from Swirl/Sinter Bronze (a,b) and Swirl/Stainless Steel Mesh Injectors (c,d) for 65 bar combustion chamber pressure, 250 K fuel temperature and 3,4 ROF

References

[1] J. Ahn, K. Ahn, and H. Y. Lim. Injection properties according to the inner shape of metal additive layer manufactured coaxial injectors. *Journal of Applied Fluid Mechanics*, 15(4), jul 2022.

[2] J. M. Beer and N. A. Chigier. Combustion aerodynamics. *Applied Science, London, UK*, 1972.

[3] Jan Deeken, Dmitry Suslov, Oskar Haidn, and Stefan Schlechtriem. Combustion efficiency sensitivity studies of the API injector concept. In *49th AIAA Aerospace Sciences Meeting including the New Horizons Forum and Aerospace Exposition*. American Institute of Aeronautics and Astronautics, 2011.

[4] B. Ivancic and W. Mayer. Time- and length scales of combustion in liquid rocket thrust chambers. *Journal of Propulsion and Power*, 18(2):247–253, mar 2002.

[5] J. Lux and O. Haidn. Flame stabilization in high-pressure liquid oxygen/methane rocket engine combustion. *J. Propul. Power 25*, 2009.

[6] I. F. Macdonald, M. S. El-Sayed, K. Mow, and F. A. L. Dullien. Flow through porous media - the ergun equation revisited. *Ind. Eng. Chem. Fundam., Vol. 18, No. 3*, 1979.

[7] Wolfgang Mayer and Hiroshi Tamura. Propellant injection in a liquid oxygen/gaseous hydrogen rocket engine. *Journal of Propulsion and Power*, 12(6):1137–1147, nov 1996.

[8] Douglas Ruth and Huiping Ma. On the derivation of the forchheimer equationby means of the averaging theorem. *Transport in Porous Media 7: 255-264.*, 1992.

[9] B. E. Schmidt. Compressible flow through porous media with application to injection. 2015.

[10] Fahd Siddiqui and Mohamed Y. Soliman. Non-darcy skin effect with a new boundary condition. *International Journal of Petroleum and Petrochemical Engineering (IJPPE)*, 2017.

[11] Joshua J. Smith, Gerald Schneider, Dmitry Suslov, Michael Oschwald, and Oskar Haidn. Steady-state high pressure LOx/h2 rocket engine combustion. *Aerospace Science and Technology*, 11(1):39–47, jan 2007.

[12] Dimitry Suslov, Jan Deeken, and Oskar Haidn. Investigation of the API-injection concept in a LOX/LH2 combustion chamber at GG/PB operation conditions. In *48th AIAA/ASME/SAE/ASEE Joint Propulsion Conference*. American Institute of Aeronautics and Astronautics, 2012.

DOI: 10.13009/EUCASS2023-031

[13] Dmitry I. Suslov, Justin S. Hardi, and Michael Oschwald. Full-length visualisation of liquid oxygen disintegration in a single injector sub-scale rocket combustor. *Aerospace Science and TechnologyVolume 86, Pages 444-454*, 2019.